Atmos. Chem. Phys. Discuss., 7, 3901–3939, 2007
www.atmos-chem-phys-discuss.net/7/3901/2007/

Atmospheric Chemistry and Physics Discussions

Understanding the formation of biogenic secondary organic aerosol from α-pinene in smog chamber studies: role of organic peroxy radicals

B. Bonn[1,*], **H. Korhonen**[2], **T. Petäjä**[1], **M. Boy**[1], **and M. Kulmala**[1]

[1]Department of Physical Sciences, University of Helsinki, Helsinki, Finland
[2]School of Earth and Environment, University of Leeds, Leeds, UK
[*]now at: Department of Plant Physiology, Estonian University of Life Sciences, Tartu, Estonia

Received: 19 February 2007 – Accepted: 14 March 2007 – Published: 21 March 2007

Correspondence to: B. Bonn (boris.bonn@helsinki.fi)

Abstract

This study focusses on the description of the nucleation process observed during the ozone reaction of the biogenic monoterpene α-pinene in smog chambers. Therefore, a detailed aerosol dynamics model (UHMA) was extended by a tropospheric chemistry module and a detailed description of the first steps of organic nucleation. We assume secondary ozonides to act as nucleation initiating molecules, which are subsequently activated by reactions with organic peroxy radicals (RO_2). With this set-up the observed particle size distributions of an exemplary experiment in Valencia was reproduced, when only the long-lived organic compounds like carboxylic acids and carbonyl compounds are detected by the available aerosol size distribution instruments. Our results indicate that fragile or reactive species might get destroyed because of weak bond breakage during the size classification. This assumption would imply a serious detection problem in nucleation studies to be solved.

1 Introduction

New aerosol particle formation from the oxidation of biogenic volatile organic compounds has been observed in a multitude of smog chamber studies (Seinfeld and Pandis, 1998; Kamens et al., 1999; Koch et al., 2000; Hoffmann, 2002). However, the explanation by homogeneous nucleation (Seinfeld and Pandis, 1998) of a single non-volatile oxidation product such as dicarboxylic acids seems to fail in reproducing the onset of nucleation observed (Kamens et al., 1999). This is caused by insufficient gas-phase concentrations and the slow production of the compounds currently known. Even when applying the highly detailed degradation scheme of the Master Chemical Mechanism (MCM, Jenkin et al., 1997, 2000) for the oxidation of α-pinene with about 500 products and 1550 reactions involved, the estimated liquid phase saturation vapour pressures of all considered products had to be reduced by a factor of 120 to reproduce the aerosol volume observed (Jenkin, 2004). However, the vapour pressures of known

ACPD

7, 3901–3939, 2007

organic compounds are insufficient to initiate homogeneous nucleation (Kamens et al., 1999). Additionally, there is evidence for the occurrence of heterogeneous reactions at the surface of or inside the aerosol-phase, causing the formation of larger products with lower saturation vapour pressures (Jang et al., 2002; Kalberer et al., 2004; Zhang et al., 2004; Doherty et al., 2005). On the contrary, the exact heterogeneous processes occurring are unknown, because most of the suggested reactions are disproven to be relevant by Barsanti and Pankow (2004). This leads to a dilemma, when aiming at describing and understanding the formation process even for smog chamber studies. It becomes even worse, when the results obtained in smog chambers are extrapolated to ambient conditions in order to understand ambient nucleation events and atmospheric aerosol formation processes.

Nevertheless, it is reasonable to assume that the current knowledge of the gas-phase reactions is accurate. There are also indications that the present ratio of peroxy radicals, in detail hydroperoxy (HO_2) and organic peroxy radicals (RO_2), has a strong impact on the amount of aerosol formed (Tolocka et al., 2006). Consequently, there seems to be a different mechanism of new aerosol particle formation from gaseous organic precursors as for the homogeneous approach with gaseous non- and semi-volatile organic compounds to condense on. This study aims to explain this alternative way for organics at least for smog chamber conditions. But it might be applicable for atmospheric conditions too.

2 Methods

2.1 Simulation

For theoretical studies the University of Helsinki Multicomponent Aerosol box model (UHMA) (Korhonen et al., 2004) was used and extended by a chemical degradation scheme. The UHMA model includes the detailed description of the physical processes of the present aerosol size distribution between 0.35 and 500 nm in cluster or particle

radius. For existing clusters or particles these are growth and loss by collision, coalescence and condensation. Additionally particles are removed by dry deposition. Please see Korhonen et al. (2004) for further details on the individual representation within the model. For smog chamber conditions the size dependent aerosol particle loss rate by Takekawa et al. (2003) was applied in this study. Because of the treatment of ambient conditions involving sulphuric acid only, the nucleation mechanism described by Korhonen et al. (2004) focussed on three different schemes for sulphuric acid as nucleation initiator, i.e. binary and ternary nucleation as well as kinetic nucleation, limited by the collision frequency of two sulphuric acid molecules.

Since this approach is not considerable in pure organic smog chamber studies without gaseous or aerosol-phase sulphuric acid present, we formulated a different pure organic nucleation scheme, which is described in the following.

2.1.1 Organic nucleation

Based on the findings of Kamens et al. (1999), Bonn et al (2002) and Tolocka et al. (2006) the nucleation scheme starts by the formation of secondary ozonides as initial nucleation nuclei. These are formed earliest in the oxidation of α–pinene by ozone from the reaction of the stabilised Criegee biradical (sCI) with carbonyl compounds (Calvert et al., 2000):

$$\alpha - \text{pinene} + O_3 \rightarrow \text{primary ozonide} \quad (1)$$

$$\text{primary ozonide} \rightarrow 0.125\ \text{sCI} + 0.875\ \text{HP channel} \quad (2)$$

$$\text{sCI} + H_2O \rightarrow \text{hydroxy} - \text{hydroperoxide} \quad (3)$$

$$\rightarrow \text{pinonaldehyde} + H_2O_2 \quad (4)$$

$$\text{sCI} + \text{carbonyl} \rightarrow \text{secondary ozonide} \quad (5)$$

To know the formation rate of the nucleation nuclei, there is a need to know the concentration of the major carbonyl compounds and the sCIs. sCIs are formed from the decomposed primary ozonides (POZ, Eq. 2), which are partly stabilised by collisions

(transfer of excess energy) with unreactive ambient gas molecules, i.e. mainly nitrogen and oxygen. The other decomposed POZs form either an unsaturated hydroperoxide (hydroperoxide channel (HP channel), OH production) or an ester (ester channel). Usually the ester channel is assumed to be of minor importance. The hydroperoxide channel is believed to be responsible for the subsequent formation of OH. Both pathways, i.e. hydroperoxide and ester channel are considered to form condensable molecules, such as e.g. pinic acid within the hydroperoxide channel (Jenkin et al., 2000; Winterhalter et al., 2000), but not nucleating molecules (Bonn et al, 2002; Bonn and Moortgat, 2002, 2003).

Similar to the work of Kamens et al. (1999) and in accordance to the experimental findings of Bonn et al (2002) and Tolocka et al. (2006) the most likely secondary ozonide to initiate the nucleation process is the one formed in the reaction of sCI with pinonaldehyde, a complex C_{20}-molecule. Although its large size – it might be around 0.95 nm in mass diameter – and the already reduced Kelvin effect, which is evidently critical for organic compounds, we do not assume homogeneous nucleation to occur in here. This is caused by two effects of secondary ozonides: (a) They are no long-lived compounds such as for example dicarboxylic acids, but rather reactive with other gas-phase compounds. (b) The lifetime due to decomposition or photolysis might be short (<20 min, Jenkin, 2005, or more likely even less). Here we assume decomposition to occur, during collisions with any possible reaction partner of the sCI (steady state assumption).

The list of possible reaction candidates is long. Their reaction rate constants with the stabilised Criegee intermediate are commonly reported relative to the one with water vapour (Reaction 3), because of the easier measurement technique and the high amounts of water present, which are easier to quantify.

To give an overview about the individual compound classes and their reactivities with the sCI, a summary of relative rates is given in Table 1. For example sCIs are found to react about 140 000–17 000 times faster with carboxylic acids than with water, aldehydes between 700 and 1000 times faster and ketones between 60–100 times faster.

Here we used the value of 14 000 for monocarboxylic acids, 17 000 for dicarboxylic acids, 1000 for aldehydes and 70 for ketones.

Reaction 3 is assumed to be the dominant sink term for sCIs, because of the usually high concentration of water vapour compensating the slow reaction rate. In earlier studies on the formation of the hydroxy-hydroperoxide a reaction rate constant of water vapour with the sCI was found to agree best at $10^{-17}\,\frac{\mathrm{cm}^3}{\mathrm{molecule}\cdot\mathrm{s}}$ (Großmann, 1999), which is used henceforth. However, it should be noted that published values range between 10^{-19} and $2\times10^{-15}\,\frac{\mathrm{cm}^3}{\mathrm{molecule}\cdot\mathrm{s}}$ in the available literature (see e.g. in Großmann, 1999). Nevertheless, the value of Großmann was found to agree best within our simulations too.

In general, the lifetime of the sCI in the smog chamber or in the atmosphere is given by the reciprocal sum of the products of individual reaction rate constants with the reacting compounds concentration. For laboratory studies of biogenic terpenes water vapour and carbonyl compounds are by far the most abundant reactants, if no additional alcohols or acids are added. Thus the lifetime can be simplified to:

$$\tau = \frac{1}{(k_{\mathrm{sCI}}^{\mathrm{H_2O}}\cdot[\mathrm{H_2O}] + k_{\mathrm{sCI}}^{\mathrm{aldehydes}}\cdot[\mathrm{aldehydes}] + k_{\mathrm{sCI}}^{\mathrm{ketones}}\cdot[\mathrm{ketones}] + \sum_i k_{\mathrm{sCI}}^{i}\cdot[i])} \tag{6}$$

$$\approx \frac{1}{(k_{\mathrm{sCI}}^{\mathrm{H_2O}}\cdot[\mathrm{H_2O}] + \sum k_{\mathrm{sCI}}^{\mathrm{carbonyls}}\cdot[\mathrm{carbonyls}]} \tag{7}$$

In the present case of 150 ppmv of water vapour the lifetime of sCIs τ and as we assume of the secondary ozonides will be about 25 s at the start, declining with increasing carbonyl concentration as the reaction proceeds.

2.1.2 Chemical scheme

The former UHMA boxmodel version of Korhonen et al. (2004) did not consider tropospheric chemistry in detail, but used fitted external data to provide sulphuric acid concentrations for aerosol formation processes. Here we extended the physical box model by a chemical gas-phase module, which covers all the major tropospheric reactions that are used in global chemistry transport models, namely the ozone, HO_x and NO_y reaction cycles, smaller VOCs (up to butane), major carbonyl compounds such as acetone and formaldehyde, isoprene and a single monoterpene (here: α−pinene). The reactions can be found in Bonn et al. (2005) and references therein. Additionally to the global simulations we extended the chemical scheme by the detailed reactions of the stabilised Criegee intermediate, which is needed for describing the nucleation initiating molecule (secondary ozonide) formation. Table 2 lists the additional reactions and their reaction rate constants considered in here.

Moreover, the reactions of SO_2 to form sulphuric acid are included in the used chemistry scheme. They were used mainly for test purposes using trace amounts of SO_2 in order to check the ability of sulphuric acid induced nucleation. However, none of the performed test simulations with sulphuric acid induced nucleation could explain the nucleation observed.

In order to describe the time dependency of all the mentioned chemical compounds, a kinetic preprocessor (KPP) scheme (Sandu and Sander, 2006) was used. It creates a Jacobian matrix from the chemical mechanism outlined above and a list of chemical compounds (variables), starting with the compounds of the smallest number of dependencies and proceeding towards the compounds with the highest dependencies such as OH. The actual reaction fluxes of the Jacobian matrix are solved by the Rosenbrock 2 method. Please see Sandu and Sander (2006) for more details.

The low- and semi-volatile organic compounds considered in the gas-phase chemistry are linked to the aerosol routines describing the nucleation, condensation and deposition. For monoterpenes these were 9 oxidation compounds or compound classes

ACPD
7, 3901–3939, 2007

EGU

used by Bonn et al. (2005): pinic and pinonic acid, low-volatile (LAPHYD) and higher volatile (HAPHYD) hydroperoxides, nitrates, PAN-type compounds, pinonaldehyde, norpinonaldehyde and an important intermediate carbonyl compound (CC6CHO, see Master Chemical Mechanism (MCM) v3.1 (2007) for the structure) on the degradation pathway to finally CO_2.In order to describe nucleation in the smog chamber four additional compounds, which originate from the reactions of the stabilised Criegee intermediate (sCI) were considered: (C_{10}-hydroxyalkyl-hydroperoxide, HAHP), hydroperoxy formate, (HPAA) as well as large (C_{20}) and smaller ($\leq C_{11}$) secondary ozonides.

The considered radical species include the sCI and the different organic peroxy radicals (RO_2) formed. Because of missing thermodynamic properties for most of the products considered, saturation vapour pressures have been estimated from liquid phase boiling point temperatures as described by Jenkin (2004) for calculating partitioning between gas and aerosol-phase (Pankow, 1994a,b):

$$p_{\text{sat}} = \frac{1}{120} \cdot p_{\ominus} \cdot \exp\left(-\frac{\Delta S_{\text{vap}}}{R} \cdot \left(1.8 \cdot \frac{T_b}{T} - 1\right) - 0.8 \cdot \ln\left(\frac{T_{b,i}}{T}\right)\right). \quad (8)$$

ΔS_{vap} is the vaporization enthalpy of the compound (see Table 3). T abbreviates the present temperature in Kelvin, R the ideal gas constant of 8.3144 $\frac{\text{J}}{\text{mol·K}}$ and $p_{\ominus}$ the standard pressure of 101 325 Pascals as described by Jenkin (2004). The individual boiling point temperatures T_b were obtained by application of structure activity relationships (SAR) using the method by Joback and Reid (1987). The estimated boiling point temperatures and vaporization entropies of the used compounds are given in Table 3. All calculated saturation vapour pressures p_{sat} are finally divided by 120 as done by Jenkin (2004), because of the extrapolation from small to larger compounds within the SAR relationships and most likely due to a different liquid-like behaviour of the compounds involved in.

The partitioning process is treated dynamically as formulated by Kamens et al.

(1999) and Jenkin (2004), taking into account the flux on- and offward the individual particles. Since this was a major addition to the model structure, we renamed it to UHMA-KAS (University of Helsinki Multicomponent Aerosol model – Kemi Aerosolin Substanssit (engl: chemistry of aerosol substances) that is used in the following.

2.1.3 Activation

Next to the formation of nucleation initiating molecules (NIM's, i.e. large secondary ozonide molecules) there is a need to activate these. We assume this to happen in analogy to cloud condensation nuclei (CCN). Since water is not present in high amounts and relative humidities are usually kept low to keep surface losses on the reactor walls small, the aerosol can be assumed as dry. Any water-solubility effect of condensable gaseous products as described by the nano-Köhler theory (Kulmala et al., 2004) to lower the necessary supersaturation initiated by water-organics interaction is thus not possible. Furthermore, any water vapour present counteracts the formation of NIM's because of its competitive reaction with the stabilised Criegee intermediate.

A further possibility is the interaction of organic molecules within the aerosol phase (dissolution, nano-Köhler theory applied to organics. Earlier studies have e.g. reported acid-dimer formation (Kückelmann et al., 2000).

Non-volatile organic compounds like the carboxylic acids have two barriers to overcome in order to contribute to aerosol mass formation: the first one is the extremely high Kelvin effect for organic compounds even at about 0.9 nm in diameter. Although we might argue, if the concept of Kelvin effect is applicable on the nm-scale. Applying the Kelvin effect on a nuclei with a density of 1200 $kg\,m^{-3}$ and pinic acid at room temperature would require a supersaturation of ca. 4000. Taking the saturation vapour pressure description of Bilde and Pandis (2001) of the pure compound this yields a saturation mixing ratio of 420 pptv (solid state) and including the Kelvin effect of 1.7 ppmv. This Kelvin effect is drastically reduced by the contact angle (Fletcher, 1958) between the condensing compound and the aerosol. Depending on the solubility of the vapour molecules in the aerosol phase this can lower the supersaturation needed to about 4

ACPD
7, 3901–3939, 2007

(entirely soluble).

Even if the much smaller supersaturation because of the surface curvature effect of 4 is applied, the necessary concentration would be 1.68 ppbv. Assuming a reasonable pinic acid yield of 3 mol% (Winterhalter et al., 2000) a conversion of 56 ppbv is needed to allow activation by the dicarboxylic acid. However, in the experiment studied remarkably smaller concentrations of α-pinene were used and thus, the necessary concentration of pinic acid will neither be reached inside the smog chamber experiment nor at any atmospheric conditions at different locations and time.

Second, even when the necessary supersaturation is sufficiently small, the non-volatile compounds require time to exceed it, which is too long when comparing with observations. Semi-volatile products are even less likely to contribute to the activation.

The only remaining possibility is a reactivity and thus collision controlled activation and early growth. Zhang and Wexler (2002) pointed out this first, concluding that this is due to an acid-catalyzed reaction of organics on sulphuric acid nuclei. However, the latter is not present here.

Imagine now a reactive collision partner, for instance a radical, which interacts with the reactive nuclei or particle at one of its various functionalities such as hydroxyl groups (-OH), carbonyl groups (=O) or nitrate groups (-ONO). This will form a complex that is rather sensitive to environmental and instrumental conditions. Heat, radiation or external energy added will destroy this complex as it is well known in mass spectroscopy. Nevertheless, it is the key to cross the nucleation barrier, i.e. the size of 1–2 nm in diameter. After the decrease of the Kelvin effect to reasonably small numbers the non- and semi-volatile compounds will start to contribute by condensation onto or partitioning into the aerosol-phase via the partitioning concept of Pankow (1994b). sCI biradicals might contribute as well. But their concentration is too small for causing a major contribution because of their short lifetime compared to other radicals.

In this context, the most likely candidates are hydroperoxy (HO_2) and organic peroxy (RO_2) radicals. Both can contribute to the aerosol mass and volume, thus the growth. The reaction with hydroxyl radicals will turn any of the reactive aerosol compounds

into water soluble ones because of the formed hydroxy or hydroperoxy group. But the increase in size is much more efficient for organic peroxy radicals because of their remarkably higher molar mass. Taking into account to first stage organic peroxy radicals in the ozone reaction of α-pinene (molar mass between 171 and 199 g mol^{-1}) are about six times as large as the competing hydroperoxy radicals (molar mass = 33 g mol^{-1}). However, both peroxy radical types are relevant because they affect the speed of the following addition reaction.

The critical point is the actual heterogeneous reaction rate constant. Gas-phase reaction rate constants are measured and known for small organic peroxy radicals with NO, HO_2 and cross reactions with other organic peroxy radicals ($R'O_2$). In this study, the reaction rate constant of RO_2 with NO and HO_2 has been used as formulated within the Master Chemical Mechanism of the University of Leeds (Master Chemical Mechanism (MCM) v3.1, 2007). The used RO_2 cross reaction is taken from the decane (C_{10}-alkane) peroxy radical, which is closest to the first stage monoterpene derived RO_2. For other oxidation reactions the latter needs to be modified according to the RO_2-mixture.

$$k_{RO_2+NO} = 2.54 \times 10^{-13} \cdot \exp(360/T) \quad (9)$$

$$k_{RO_2+HO_2} = 2.91 \times 10^{-12} \cdot \exp(1300/T) \quad (10)$$

$$k_{RO_2+R'O_2} \approx 2.5 \times 10^{-13} \frac{\text{cm}^3}{\text{molecule} \cdot \text{s}} \quad (11)$$

Next to the pure gas-phase kinetic description, there is a need to extend it to larger aerosol particles with an increase in collision frequency with increasing particle size. Here we use the concept of Svante Arrhenius (Finnlayson-Pitts and Pitts, 2000). He formulated the common description of the reaction rate constant:

$$k = A \cdot \exp\left(-\frac{E_A}{RT}\right) \quad (12)$$

E_A is the necessary activation energy for the reaction to occur, R the ideal gas constant

($8.3144\ \frac{J}{K \cdot mol}$) and T the temperature.

Finnlayson-Pitts and Pitts (2000) used the kinetic collision theory to explain the meaning of the constant A. The collision approach leads to:

$$k = P \cdot \text{collision} \cdot \exp\left(-\frac{E_0}{k_B T}\right) \tag{13}$$

In there, E_0 abbreviates the molar threshold or activation energy, which is equal to $N_A \cdot E_A$, with Avogadros number N_A. k_B is used for the Boltzmann constant. Hence the product of steric factor P and the collision rate is the so-called Arrhenius factor A.

$$A = P \cdot \text{collision} \tag{14}$$

Let us now assume a reaction not by two gas-phase molecules but by one molecule and a nuclei or aerosol particle (heterogeneous). The steric factor P will not change much, since either all surface sites might be reacting with the organic peroxy radical or we can use the reacting volume fraction (assuming a well mixed nuclei). This is treated separately from the reaction rate constant in the following by an external multiplication factor. So we can formulate the heterogeneous reaction rate of RO_2 with the nuclei or aerosol particle by correcting or scaling with the different collision rate for a single aerosol constituent:

$$k_{RO_2}^{aerosol} = k_{RO_2}^{gas} \cdot \frac{\text{collision}_{RO_2}^{aerosol}}{\text{collision}_{RO_2}^{gas}} \tag{15}$$

The corrected reaction rates are increasing remarkably with size, raising by 20 000 when increasing the size of the molecule, cluster or particle from 1 to 100 nm in radius (Fig. 1). A room temperature of 298.15 K and a density of 1000 kg mol^{-1} has been used to obtain Fig. 1. However, changes in particle density did not affect the plot significantly and changes in temperature caused only minor deviations from the plot shown.

The calculated heterogenous reaction rate rises proportional to the squared radius for molecules, clusters and smallest particles smaller than about 3 nm. This increase becomes linearly dependent on the radius for larger particles. Consequently,

the growth of clusters or aerosol particles speeds up, once the first activation step is done, which is commonly observed in all smog chamber studies of secondary organic aerosol formation. If there are several compounds in the aerosol phase, as to be expected for most studies, the total rate constant is obtained by summing the three collision corrected rate constants with the fraction of the three groups, (i) acids and hydroperoxides, (ii) nitrate compounds and (iii) the remainder.

But why do these reaction products not behave like in the gas-phase, where the reaction of RO_2 and $R'O_2$ usually yields two products? Either this intermediate is rather unstable because of excess energy, it breaks up easily into two parts or the larger the formed molecule the better the energy is distributed over the entire complex, i.e. stabilises and thus prevents direct decomposition as it is found by Chuong et al. (2004) for the stabilised fraction of terpene-ozone reactions.

Here we assume the size to increase sufficient to allow stabilisation and thus formation of this complex to occur. The link between the organic peroxy radical and the nuclei or the particle compounds might consist of a $R_1C\text{-}O\text{-}O\text{-}CR_2$ structure. The weakest point of this complex is most likely either the O-O bond with a bond energy between 155–158 kJ mol^{-1} or the RC-O bond (energy $\geq$148 kJ mol^{-1}) with the latter one depending on the residuum R (Finnlayson-Pitts and Pitts, 2000; Linde, 2001). Hence, these complex molecules are not expected to be as entirely stable or long-lived products as a carboxylic acid or a carbonyl compound with bond energies much higher than the ones given.

This causes detection problems e.g. for spectroscopy and detection. Any additional energy, e.g. because of charging of aerosol particles or because of the latent heat release (condensation) in the particle counter, might destroy the complex and thus prevent detection by the present particle size distribution instruments. This feature is also common in secondary organic aerosol formation but not in nucleation of sulphuric acid aerosols (Bonn, 2002): Particles are seen from diameters above several nanometers with a gap below. The higher the initial alkene, here α–pinene, concentration and reaction rate, the more pronounced the effect appears. However, the lack of time res-

olution of the particle size distribution measurements is not able to explain this, which has been checked in flow tube studies (Bonn et al, 2002).

Additional to the increasing speed with increasing size the effect of hydroperoxy radicals (HO_2) (Tolocka et al., 2006) needs to be taken into account, which are ubiquitous in the ambient air as well as in rather high concentrations especially in smog chamber experiments. Once there are reactive organic compounds HO_2 and RO_2 (and also NO for ambient conditions) will compete in reacting with the reactive hydrocarbons. In case of HO_2 reactions hydroperoxy or acidic compounds are formed, which are subsequently interacting with the RO_2 radicals. The major impact of this focusses on the reaction speed of RO_2 with the organic aerosol components. The reaction rate of RO_2 with HO_2, NO and RO_2 are given in Eqs. (9)–(11). The reaction rate with the present nucleation nuclei can be formulated in accordance with the present concentrations of the competitors:

$$k_{RO_2}^{nuclei} = \frac{k_{RO_2}^{HO_2}[HO_2] + k_{RO_2}^{NO}[NO] + k_{RO_2}^{RO_2}[RO_2]}{[HO_2] + [NO] + [RO_2]} \quad (16)$$

And the corresponding reaction rate for larger aerosol particles will need to take into account the fractions of the individual compound classes (acids and hydroperoxides, nitrate and carbonyl compounds) assuming a well mixed aerosol-phase.

2.2 Experimental

For intercomparison with smog chamber observations with simulated smog chamber α-pinene oxidation, we used datasets of an experiment, conducted at the EUPHORE smog chamber facility (Becker, 1996; Martín-Reviejo and Wirtz, 2005) in Valencia (Spain) within the framework of the European project Origin of Secondary Organic Aerosol (OSOA, Hoffmann, 2002). The EUPHORE smog chamber B, which was used therefore, consists of a half spherical Teflon chamber with a total volume of approximately 200 m^3. For pure ozone reactions in the absence of sunlight, the chamber can be covered by a spherical roof. This was applied in our experiment.

The experiment was prepared by inserting ozone, produced by an ozone generator, until it reached its designed volume mixing inside the chamber. Subsequently, its concentration was monitored as for other gases like α−pinene, HCOOH, HNO_3, HCHO and SF_6 by Fourier-Transform Infrared spectroscopy (FT-IR, Nicolet Magna 550). In this context, 65 µL of SF_6 were injected before the start of the experiment in order to obtain the gas-phase loss rate towards the chamber walls. The loss term was obtained afterwards by fitting a first order decay of the FT-IR derived concentration of SF_6. α−pinene was measured by gas-chromatography (GC, 8000 Fisons) too. NO and NO_x concentrations were obtained by an NO/NO_2- and an NO_x-Analyzer as well as CO by a CO-monitor.

Besides of the measurements of the gaseous compound concentrations the aerosol particle size distribution was measured with a Differential Mobility Particle Sizer (DMPS, Aalto et al., 2001) by the University of Helsinki. The sample was drawn from the EUPHORE chamber using a 10 mm OD copper tubing. Prior to size classification the sampled particles were charged with a Ni-63 β source (360 MBq). The DMPS included two Differential Mobility Analyzers (DMA,Winklmayr et al., 1991) for the size range of 3–400 nm with a suitable condensation particle counter for particle detection after classification. The first Vienna type DMA classified aerosol particles the size range between 3 and 15 nm and was connected to an ultra-fine CPC (TSI 3025). The second one selected the particles with an electrical mobility derived diameter between 15 and 400 nm before counting with a TSI 3010. With this set-up the entire particle size distribution was measured with a time resolution of five minutes from the start until the termination of the α-pinene oxidation experiment. This dataset is used for intercomparison with the particle size distributions obtained by the simulations.

3 α-pinene experiment in EUPHORE

Next we apply the theoretical framework to the conditions found in a smog chamber experiment. Therefore, we used the α−pinene ozone reaction experiment conducted at

the EUPHORE smog chamber facility in Valencia (Spain) on the 15 March 2001 within the EU-project OSOA (Hoffmann, 2002). No seed aerosol was used and the smog chamber was flushed with purified synthetic air during the night before to establish clean conditions (see e.g. Zador et al., 2006). Ozone was inserted first, until it reached a volume mixing ratio of 110 ppbv. The present dew point was –42 °C, referring to a water vapour mixing ratio of about 150 ppmv at 14.7°C. Because of the ozone reaction the chamber was covered by a roof to protect sunlight to enter, the temperature increased to about 23.5°C at noon and stayed there until the experiment was terminated. This caused the volume mixing ratio of water vapour to decline after the start of the experiment.

Besides the monitoring of various chemical compounds, the particle size spectrum was measured with a DMPS (twin-DMA set-up to catch all particles between 3 and ≈500 nm in diameter), applying a time resolution of 5 min. The experiment was started by adding 13 µL of α-pinene at 10:15 a.m. and was rapidly mixed within the chamber by a fan, corresponding to an α-pinene volume mixing ratio of 9 ppbv.

After the initially added α-pinene has been oxidised almost completely (decline to about 1% of its initial value), a further injection of $\alpha-$pinene (26 µL ≙18 ppbv) was made.

The effects of the additions of α-pinene were obvious in the measured aerosol particle size distributions (Fig. 2). The first injection of $\alpha-$pinene is closely followed by the detection of a nucleation event, but obvious first at larger particle diameters (D_p >4 nm) with the appearance of the maximum number density above 20 nm. A second major feature is the change in the size distribution at the second addition. Here one can conclude that actually only a small nucleation in strength occurred, but a rather strong increase in size of the pre-existing particles, which is reasonable, since the pre-existing particles act as a strong condensation sink for low- and non-volatile compounds.

Nevertheless, an initial gap in detection between no particles at all at the start of the experiment and 5 nm in diameter remains (25 nm for the maximum intensity). This is commonly ascribed to the low time resolution by the particle size distribution measure-

ments, which would miss the onset of nucleation at smaller particle sizes.

The simulations were started by initializing the chemistry of the box model UHMAKAS with the measured initial gas-phase data of NO_x, NO, terpene and ozone mixing ratios. Measured temperature and humidity values were used throughout the entire experiment. For the aerosol-interacting organic peroxy radicals we calculated the RO_2-mixtures average molar mass $\overline{M_{RO_2}}$, molecular volume v_{molec,RO_2} and average reaction rates k_{ave} within an aerosol size section. Therefore, we weighed the individual RO_2 molar masses by their fraction of the total organic peroxy radicals (Eq. 17). The average reaction rates k_{ave} of the organic peroxy radicals with the aerosol particle of interest were obtained by multiplying the collision corrected reaction rate constants for the three different type of reactions (HO_2 + RO_2, RO_2 + NO and RO_2 + $R'O_2$) with the individual aerosol volume fractions of three groups:

(i) hydroperoxy compounds
acids, hydroperoxides → HO_2 + RO_2,

(ii) nitrate compounds:
nitrates, PAN type species → RO_2 + NO and

(iii) the remaining:
secondary ozonides, carbonyl compounds → RO_2 + $R'O_2$) (see Eq. 19).

$$\overline{M_{RO_2}} = \sum_i \frac{[RO_{2,i}]}{[RO_2]} \cdot M_i \tag{17}$$

$$v_{molec,RO_2} = \frac{\overline{M_{RO_2}}}{N_A \cdot \rho_i} \tag{18}$$

$$k_{ave} = \sum_i k^{aerosol}_{RO_2+X_i} \cdot \frac{v_{part,X_i}}{v_{part}} \tag{19}$$

ACPD
7, 3901–3939, 2007

From this we get the increase of the individual aerosol particle per time step Δt:

$$\frac{\Delta v_{\text{part}}}{\Delta t} = \sum_i k_{\text{ave},i} \cdot \overline{[\text{RO}_2]} \cdot v_{\text{molec,RO}_2} \quad (20)$$

The obtained 'averaged' reaction rate constant for the specific aerosol size was then multiplied with the summed RO_2 concentration and average molecular mass to get the volume increase. The organic peroxy radicals used were derived from the Mainz Alpha-pinene Mechanism (MAM) (Bonn et al., 2005).

By doing so, we simulated the nucleation events and their individual evolutions, including the particle composition. For the latter we need to assume an identical composition for all particles inside a size section, which is questionable e.g. under atmospheric conditions.

4 Results

4.1 Particle size distributions

When studying the results obtained by the simulation, it is clear that the time of both nucleation events is simulated by UHMA-KAS (Fig. 3) in agreement with the DMPS measurements (Fig. 2). The second injection of α-pinene resulted both in growth of the pre-existing particle population and formation of a new particles. Herein, the pre-existing particles act as a strong sink of condensable organic vapours.

However, there are some differences apparent:

1. The simulated nucleation events start at the molecular size level, while the observed maximum in number size distribution becomes apparent at sizes larger than 10 nm in diameter.

2. The intensity of the simulated events is higher than of the measured ones.

The first difference might be in agreement with the earlier suggestion that the time resolution of the DMPS measurements is too coarse to obtain the very early stage of nucleation and because of that the smallest particles cannot be detected. But the model output is set to exactly the same output frequency as the instrument. So where do the particles come from, in case they become visible first at about 10 nm in diameter, which is already an enormous mass assuming a density of 1000 kg m^{-3} (5.24×10^{-19} g)? There is no maximum in number size distribution observed, which appears at smaller sizes and is shifted to larger sizes by growth.

To explain the differences between simulation and observation, the modelled aerosol size distribution was divided into a "reactive" and an entirely "stable" aerosol fraction by taking into account the chemical composition of the aerosol particles within a size section. In particular, the stable compounds are assumed to be carboxylic acids, carbonyl compounds and nitrates. Therefore, an aerosol particle is assumed to be detected by the DMPS instrument only, if the stable aerosol fraction of the particle is larger than the lower section size. For this we assumed the radical derived part of the aerosol particle to be destroyed by the detection method. This might occur by either the very strong charge interactions during the bipolar charging for DMA analysis or by the release of latent heat of the condensing compound within the particle counter. For example, if butanol is used as the condensing liquid for the condensation particle counter, the cluster or particle needs to survive the transfer of the formation energy of a critical cluster, which further grows to be detected by the counter optics. This formation energy release is sufficient to destroy about 25 O-O bonds. If we consider the major RO_2 molecules to have a molar mass of about 185 g mol^{-1}, this corresponds to a loss of 25×185 g mol^{-1} and thus about 4600 amu.

The assumption of a fragile fraction of the aerosol particles during detection affected the width of the modelled distribution and reduced the concentration below 10 nm in particular (Fig. 3) because of the small bin size.

4.2 Stable compound contribution to aerosols

Therefore, a key information to study the influence of aerosol constituents on particle size distribution measurements is the fraction of "stable" products. For the stable compounds such as carboxylic acids and carbonyl compounds this starts already at the nuclei level but increases significantly, until the contribution reaches a "steady state" at about 10 nm in diameter (Fig. 4). This observation was made by plotting the volume of "stable" aerosol compounds to the total aerosol volume for each size bin. Figure 4 displays the results at different times (lines) during the simulation. A clear change can be seen from below to above 10 nm in particle diameter. That indicates the inability of further condensable species to activate the NIM's. They mainly partition at sizes with an reduced Kelvin effect and stabilise the particles to allow detection. In any case a significant fraction even above 10 nm in diameter is simulated to be fragile. This effect might be able to explain the appearance of maximum particle number densities first at larger sizes than about 10 nm for organics (e.g. in Fig. 2), depending on the size and functionality of the used VOC.

For chemical identification this problem appears too. However, at the sizes of the highest influence of the "fragile" compounds chemical analysis is usually not carried out, since aerosol chemical analysis requires sufficient aerosol mass to be analyzed. Consequently, the chemical composition is rarely known below 10 nm in diameter (Tolocka et al., 2006) but usually much above. However, a notable fraction of the organic aerosol seems to consist of reactive matter, e.g. noted by the recent publications on heterogeneous reactions and oligomerization. Maybe this reactive driven condensation contributes significantly to the observations with respect to oligomerization.

A further effect of a fragile fraction possibly destroyed during analysis is the change of the equilibrium between gas and aerosol phase. From the partitioning theory (Pankow, 1994b; Odum et al., 1996) it is known that the larger the organic mass the more of the gas-phase species will be taken up by the aerosol particles. If a significant fraction of the organic mass is removed, a new equilibrium with even less organic aerosol matter

ACPD
7, 3901–3939, 2007

EGU

will result.

4.3 Particle number concentration

When studying the particle number concentrations above 3 nm in diameter (N_3), it can be seen that the box model predicts a similar number concentration behaviour as observed (Fig. 5, upper plot). The upper plot displays the results using the actual monoterpene injections and resulting concentrations assuming instantaneous mixing throughout the entire chamber volume. The red line indicating the stable aerosol number concentration corresponds to the number of particles remaining above 3 nm in diameter after removing the reactive fraction. The lower plot indicates the effect of delayed mixing of the injected monoterpene (assumption: 11.5 ppbv at the start). Note that in both plots the simulated number concentration was reduced to allow a better intercomparison. The time of nucleation start is identical for both α–pinene additions during the experiment. Even the different magnitudes are captured well.

Therefore, differences observed between simulated and measured total number concentrations can be explained by three different issues:

(i) The injection of the monoterpene is not instantaneously but takes some time for equilibration over the chamber volume (compare upper and lower plot in Fig. 5). During this the local concentration close to the inlet is higher leading to a speed up in particle formation (Fig. 5, lower plot) and faster reduction of the monoterpene, until the gases are mixed homogeneously. These initial particles are situated closer to the wall with the consequence of a higher deposition, which is even increased by the following fact: Usually the injected monoterpene is heated up, to enhance vaporization of the liquid added.

(ii) The lifetime of the sCI is critical in this context. The longer the lifetime the higher the possibility to get activated and thus the larger particle number will be formed. We assumed a lifetime of about 4 s that lead to reasonable results concerning the magnitude between both additions. However, a heated injection will enhance the

excess energy of the initially formed primary ozonides and reduce the stabilised fraction to smaller than 0.1 due to a need for a larger energy transfer before rearrangement to an unsaturated hydroperoxide or ester (see Eq. 2).

(iii) The activation reaction rates of RO_2 radicals with the nucleation nuclei and the subsequent growth are only estimated from available compounds smaller than those investigated here. Hence, a slightly smaller activation, let's say by a factor of 1.5 will cause a significant change in the results. These topics remain to be clarified in future studies.

4.4 Impact of HO_2 and NO_x

A further important aspect is the impact of elevated HO_2 and NO_x concentrations on secondary organic aerosol formation. This influence is well established for secondary organic aerosol formation (Seinfeld and Pandis, 1998; Presto et al., 2005). Since we assume the initial aerosol nuclei to be reactive with RO_2 they will certainly react with these too. Reactions with HO_2 will form a hydroperoxy group, the NO-reaction a nitrate group and the reaction with NO_2 might form a PAN-type compound, which we associate with the group of nitrate compounds. Once these products are formed, we can progress with the RO_2 chemistry as outlined above, but we have to take into account the change in aerosol composition and of the reaction rate. Since RO_2-HO_2 reactions are significantly faster than the organic peroxy radical self-reactions, the process of growth is likely to speed up in enhanced [HO_2] conditions. The higher the HO_2/RO_2 ratio the faster the growth process, until it reaches a saturation level, when all nuclei are turned into hydroxy- or hydroperoxy group compounds.

Additionally, there will be a difference instability of the aerosol nuclei or small aerosol particle too. The situation of the present situation in the experiment is simulated in Fig. 6. Short after the first injection the RO_2 radicals reach a maximum by far larger than the concentration of HO_2. Here the slower reaction rate of the organic peroxy radical cross-reactions comes into play. The growth process is somewhat slower and

further organic non-volatile matter can condense or partition much longer during the growth process until 100 nm in diameter.

Subsequently, RO_2 concentration decreases because of its smaller lifetime and the decline of the monoterpene oxidation rate by ozone (smaller source term). By contrast the situation is different for the second α−pinene addition: Although the RO_2 radical concentrations increase again, the present HO_2 from earlier products and from the higher monoterpene addition gets more important. The ratio of $[HO_2]/[RO_2]$ indicates this clearly (Fig. 6 (lower plot)).

4.5 Stabilised Criegee Intermediate concentrations

Finally let's take a look on the concentration and evolution with time of the most relevant compounds for this nucleation process, i.e. the stabilised Criegee biradicals. Their estimated concentration is shown in Fig. 7 in pptv. However, it should be noted that the lifetime of these biradicals is rather uncertain and will impact on the total concentration remarkably. Nevertheless, the used value of 25 s and the time evolution lead to reasonable results. A decrease in the lifetime will cause the concentration of sCIs and subsequently of activated nuclei to decrease. However, the same temporal pattern will be observed. Since the reaction rate of sCIs with water vapour is much more uncertain, we excluded sensitivity studies here. Although this indicates the decrease in number concentration, any result obtained depends strongly on the reaction rate of sCIs with water.

Moreover, the effect of delayed mixing can be seen by intercomparing the left (measured gas phase concentrations of α−pinene) and the right plot (elevated initial concentration by 30%. It seems likely that during injection of α-pinene a cloud of elevated vapour concentrations forms before it is being diluted by the fans.

5 Conclusions

Based on our results it seems plausible that large secondary ozonides are capable to initiate new particle formation by secondary organic compounds. Their predominant role is to provide a huge, reactive molecule that allows reactive uptake of further compounds, thus acting as a nucleation initiating molecule. On the other hand peroxy radicals (HO_2 and RO_2) are likely the key compounds in activating these secondary ozonide molecules at least in the laboratory experiments. By forming an fragile still reactive complex the nuclei grow, until the Kelvin effect gets sufficiently small and the condensable species concentration sufficiently large to allow condensation and partitioning. This effect will be less pronounced for large aerosol precursors, e.g. sesquiterpenes, whose products have sufficiently low vapour pressures and the production is really effective to decrease the initial diameter to overcome for condensation and partitioning. This might lower the stable cut-off diameter for detection from 10 to about 5 nm.

On the other hand, this effect will be obvious for small VOC precursors such as the anthropogenic ones, e.g. toluene or benzene. Since these are mainly oxidised by OH a huge reservoir of organic peroxy radicals is available e.g. in urban areas. This leads to the interesting interaction between different VOCs in aerosol formation: the combined effort of the common VOC mixture in ambient air seems to be rather efficient: small concentrations of large nucleation nuclei from e.g. biogenic sources or sulphuric acid and high concentrations of peroxy radicals associated with the OH oxidation of VOCs. This is a topic to be discussed in a future study.

Acknowledgements. The authors would like to thank their colleagues at EUPHORE in Valencia Spain and the colleagues within the EU project OSOA (EVK2-CT-1999-00016) for the data obtained. Additionally many colleagues at the University of Helsinki are acknowledged for support and discussion. The BACCI project is gratefully acknowledged for financial support.

References

Aalto, P., Hämeri, K., Becker, E., Weber, R., Salm, J., Mäkelä, J. M., Hoell, C., O'Dowd, C. D., Karlsson, H., Hansson, H. C., Väkevä, M., Koponen, I. K., Buzorius, G., and Kulmala, M.: Physical characterization of aerosol particles during nucleation events, Tellus, 53, 344–358, 2001. 3915

Atkinson, R.: Gas-phase tropospheric chemistry of volatile organic compounds: 1. Alkanes and alkenes, J. Phys. Chem. Ref. Data, 26, 215–290, 1997. 3931

Barsanti, K. C. and Pankow, J. F.: Thermodynamics of the formation of atmospheric organic particulate matter by accretion reactions - Part 1: Aldehydes and ketones, Atmos. Environ., 38, 4371–4382, 2004. 3903

Becker, K. H. (Ed.): The European Photoreactor EUPHORE: Design and technical development of the European Photoreactor and First Experimental Results, Final report. EU project, Bruxelles, 1996. 3914

Bilde, M. and Pandis, S. N.: Evaporation rates and vapor pressures of individual aerosol species formed in the atmospheric oxidation of α- and β-pinene, Environ. Sci. Technol., 35, 3344–3349, 2001. 3909

Bonn, B., Schuster, G., and Moortgat, G. K.: Influence of water vapor on the process of new particle formation during monoterpene ozonolysis, J. Phys. Chem. A, 106, 2869–2881, 2002. 3904, 3905, 3914

Bonn, B. and Moortgat, G. K.: New particle formation during α- and β-pinene oxidation by O_3, OH and NO_3, and the influence of water vapour: Particle size distribution studies, Atmos. Chem. Phys., 2, 183–196, 2002. 3905

Bonn, B.: Bestimmung der Größenverteilung von sekundären organischen Aerosolen in der Oxidation biogener Terpene. Ph.D. thesis, Mainz University, Mainz, 2002. 3913, 3930

Bonn, B., and Moortgat, G. K.: Sesquiterpene ozonolysis: Origin of atmospheric new particle formation from biogenic hydrocarbons, Geophys. Res. Lett., 30, 1585, doi:10.1029/2003GL0017000, 2003. 3905

Bonn, B., Schuster, G., and Moortgat, G. K.: Influence of water vapor on the process of new particle formation during monoterpene ozonolysis, J. Phys. Chem. A, 106, 2869–2881, 2002.

Bonn, B., von Kuhlmann, R., and Lawrence, M. G.: Influence of biogenic secondary organic aerosol formation approaches on atmospheric chemistry. J. Atmos. Chem., 51, 235–270, 2005. 3907, 3908, 3918, 3931

Calvert, J. G., Atkinson, R., Kerr, J. A., Madronich, S., Moortgat, G. K., and Yarwood, G.: The mechanisms of atmospheric oxidation of the alkenes. Oxford Univ. Press, New York, 2000. 3904

Chuong, B., Zhang, J., and Donahue, N. M.: Cycloalkene ozonolysis: collisionally mediated mechanistic branching, J. Am. Chem. Soc., 126, 12 363–12 373, 2004. 3913

Doherty, K. S., Wu, W., Bin Lim, Y., and Ziemann, P. J.: Contributions of organic peroxides to secondary aerosol formed from reactions of monoterpenes with O_3, Environ. Sci. Technol., 39, 4049–4059, 2005. 3903

Finnlayson-Pitts, B. and Pitts, J. N.: Chemistry of the upper and lower atmosphere. Second Edition, Academic Press, New York, 2000. 3911, 3912, 3913

Fletcher, N. H.: Size effect in heterogeneous nucleation, J. Chem. Phys., 29, 572–576, 1958. 3909

Großmann, D.: Die Gasphasenozonolyse von Alkenen in Gegenwart von Wasserdampf als Quelle für Wasserstoffperoxid und organische Peroxide in der Atmosphäre. Ph.D. thesis, Mainz University, Mainz, 1999. 3906, 3930, 3931

Hatakeyama, S. and Akimoto, H.: Mechanism for the oxidation of SO_2 in the atmosphere by the intermediate formed in ozone-olefin reactions – reaction of the adduct with water-vapor, Nippon Kagaku Kaishi, 7, 785–787, 1992. 3930

Hatakeyama, S., and Akimoto, H.: Reactions of Criegee intermediates in the gas phase, Res. Chem. Intermed., 20, 503–524, 1994. 3930

Hoffmann, T. (Ed.): Origin and formation of secondary organic aerosol, Final report. EU project, Bruxelles, 2002. 3902, 3914, 3916

Jang, M., Czoschke, N. M., Lee, S., and Kamens, R. M.: Heterogeneous atmospheric aerosol production by acid catalyzed particle-phase reactions, Science, 298, 814–817, 2002. 3903

Jayne, J. T., Pöschl, U., Chen, Y., Dai, D., Molina, L. T., Worsnop, D. R. Kolb, C. E., and Molina, M. J.: Pressure and temperature dependence of the gas-phase reaction of SO_3 with H_2O and the heterogeneous reaction of SO_3 with $H_2OH_2SO_4$ surfaces, J. Phys. Chem. A,, 101, 10 000–10 011, 1997. 3931

Jenkin, M., Saunders, S. M., and Pilling, M. J.: The tropospheric degradation of volatile organic compounds: A protocal for mechanism development, Atmos. Environ., 31, 81–104, 1997. 3902, 3931

Jenkin, M. E.: Modelling the formation and composition of secondary organic aerosol from α- and β-pinene ozonolysis using MCM v3. Atmos. Chem. Phys., 4, 1741–1757, 2004. 3902,

3908, 3909
Jenkin, M. E.: personal communication, 2005. 3905
Jenkin, M. E., Shallcross, D. E., and Harvey, J. N.: Development and application of a possible mechanism for the generation of *cis*-pinic acid form the ozonolysis of α- and β-pinene, Atmos. Environ., 34, 2837–2850, 2000. 3902, 3905
Joback, K. G. and Reid, R. C.: Estimation of pure-component properties from group contributions, Chem. Eng. Commun., 57, 233–243, 1987. 3908
Kalberer, M., Paulsen, D., Sax, M., Steinbacher, M., Dommen, D., Prevot, A. S. H., Fisseha, R., Weingartner, E., Frankevich, V., Zenobi, R., and Baltensperger, U.: Identification of polymers as major components of atmospheric organic aerosols, Science, 303, 1659–1662, 2004. 3903
Kamens, R., Jang, M., Chien, C.-J., and Leach, K.: Aerosol formation from the reaction of α-pinene and ozone using a gas-phase kinetics-aerosol partitioning model, Environ. Sci. Technol., 33, 1430–1438, 1999. 3902, 3903, 3904, 3905, 3908
Koch, S., Winterhalter, R., Uherek, E., Kolloff, A., Neeb, P., and Moortgat, G. K.: Formation of new particles in the gas phase ozonolysis of monoterpenes, Atmos. Environ., 34, 4031–4042, 2000. 3902
Korhonen, H., Lehtinen, K. E. J., and Kulmala, M.: Aerosol dynamics model UHMA: Model development and validation, Atmos. Chem. Phys., 4, 757–771, 2004. 3903, 3904, 3907
Kückelmann, U., Warscheid, S., and Hoffmann, T.: On-line characterization of organic aerosols formed from biogenic precursors using atmospheric pressure chemical ionization mass spectrometry, Anal. Chem., 72, 1905–1912, 2000. 3909
Kulmala, M., Kerminen, V.-M., Anttila, T., Laaksonen, A., and O'Dowd, C.: Organic aerosol formation via sulphate cluster activation, J. Geophys. Res. (Atmos.), 109, D04205 doi:10.1029/2003JD003961, 2004. 3909
Linde, D. R. (Ed.): CRC Handbook of chemistry and physics, 82nd ed., CRC Press, Boca Raton, 2001. 3913
Martín-Reviejo, M. and Wirtz, K.: Is benzene a precursor for secondary organic aerosol?, Environ. Sci. Technol., t39, 1045–1054, 2005. 3914
Master Chemical Mechanism (MCM) v3.1: http://mcm.leeds.ac.uk/MCM/, 2007. 3908, 3911, 3931
Neeb, P., Horie, O., and Moortgat, G. K.: The ethene-ozone reaction in the gas-phase, J. Phys. Chem., 102, 6778–6785, 1996a. 3930

Neeb, P., Sauer, F., Horie, O., and Moortgat, G. K.: Formation of hydroxymethyl hydroperoxide and formic acid in alkene ozonolysis in the presence of water vapour, Atmos. Environ., 31, 1417–1423, 1996b. 3930

Odum, J. R., Hoffmann, T., Bowman, F., Collins, D., Flagan, R. C., and Seinfeld, J. H.: Gas/particle partitioning and secondary organic aerosol yields, Environ. Sci. Technol., 30, 2580–2585, 1996. 3920

Pankow, J. F.: An absorption model of gas/aerosol partitioning organic compounds in the atmosphere, Atmos. Environ., 28, 185–188, 1994a. 3908

Pankow, J. F.: An absorption model of the gas/aerosol partitioning involved in the formation of secondary organic aerosol, Atmos. Environ., 28, 189–193, 1994b. 3908, 3910, 3920

Presto, A. A., Huff Hartz, K. E., and Donahue, N. M.: Secondary organic aerosol production from terpene ozonolysis: 2. effect of no_x concentration, Environ. Sci. Technol., 39, 7046–7054, 2005. 3922

Sandu, A., and Sander, R.: Technical note: Simulating chemical systems in Fortran90 and Matlab with the Kinetic PreProcessor KPP-2.1, Atmos. Chem. Phys., 6, 187–195, 2006. 3907

Schäfer, C.: Mechanistische Studien zur Gasphasen-Ozonolyse einfacher Alkene – Konsequenzen für das Oxidationspotential der Troposphäre. Ph.D. thesis, Mainz University, Mainz, Germany, 1997. 3930

Seinfeld, J. H. and Pandis, S. N.: Atmospheric chemistry and physics. Wiley Interscience, New York, 1998. 3902, 3922

Su, F., Calvert, J. G., and Shaw, J. H.: A FTIR spectroscoic study of the ozone-ethene reaction mechanism in O_2-rich mixtures, J. Phys. Chem., 84, 239–246, 1980. 3930

Takekawa, H., Minoura, H., and Yamazaki, S.: Temperature dependency of secondary organic aerosol formation by photo-oxidation of hydrocarbons, Atmos. Environ., 37, 3413–3424, 2003. 3904

Tobias, H. J. and Ziemann, P. J.: Kinetics of the gas-phase reactions of alcohols, aldehydes, carboxylic acids and water with the C_{13} Criegee intermediate formed from the ozonolysis of 1-tetradecene, J. Phys. Chem. A, 105, 6129–6135, 2001. 3930

Tolocka, M. P., Heaton, K. J., Dreyfus, M. A.,Wang, S., Zordan, C. A., Saul, T. D., and Johnston, M. V.: Chemistry of particle interception and growth during α-pinene ozonolysis, Environ. Sci. Technol., 40, 1843–1848, 2006. 3903, 3904, 3905, 3914, 3920

Winklmayr, W., Reischl, G. P., Lindner, A. O., and Berner, A.: A new electromobility spectrome-

ter for the measurement of aerosol size distributions in the size range from 1 to 1000 nm, J. Aerosol Sci., 22, 289–296, 1991. 3915

Winterhalter, R., Neeb, P., Grossmann, D., Kolloff, A., Horie, O., and Moortgat, G. K.: Products and mechanism in the gas-phase reaction of ozone with β-pinene, J. Atmos. Chem., 35, 165–197, 2000. 3905, 3910

Zador, J., Turanyi, T., Wirtz, K., and Pilling, M. J.: Measurement and investigation of chamber radical sources in the European Photoreactor (EUPHORE), J. Atmos. Chem., 55, 147–166, 2006. 3916

Zhang, K. M. and Wexler, A. S.: A hypothesis for growth of fresh atmospheric nuclei, J. Geophys. Res., 107(D21), 4577, doi:10.1029/2002JD002180, 2002. 3910

Zhang, R., Suh, I., Zhao, J., Zhang, D., Fortner, E. C., Tie, X., Molina, L. T., and Molina, M. J.: Atmospheric new particle formation enhanced by organic acids, Science, 304, 1487–1490, 2004. 3903

Table 1. Relative rate constants for the reaction of different compounds with the stabilised Criegee intermediate compared to the one of water vapour (Großmann, 1999).

compound	$\frac{k^{i}_{sCI}}{k^{H_2O}_{sCI}}$	reference
carboxylic acids	14 000–17 000	Neeb et al. (1996b); Tobias and Ziemann (2001); Bonn (2002)
aldehydes	700–1000	Neeb et al. (1996a); Bonn (2002)
ketones	60–100	
alcohols	22–50	Tobias and Ziemann (2001)
CO	8	Su et al. (1980)
alkanes	38-59	estimated from Schäfer (1997)
SO_2	170	Hatakeyama and Akimoto (1992)
NO	610	Hatakeyama and Akimoto (1994)
NO_2	61	Hatakeyama and Akimoto (1994)
O_3	11	Su et al. (1980)

Table 2. Reactions added to the MAM-scheme (Bonn et al., 2005). T abbreviates temperature, M the total gas-molecule concentration and the shortening of the compounds is given in the text, where it is not apparent. The reaction rate constant of stabilised Criegee intermediates (sCI) with water vapour is assumed to be $10^{-17}\ \frac{cm^3}{molecule\cdots}$.

reaction	reaction rate constant
α−pinene + O_3 → 0.1 sCI + 0.6 C1079O2 + 0.27 C96O2 + 0.27 CO + 0.03 pinonic acid + 0.87 OH	$1.01 \times 10^{-15} \cdot \exp(-732/T)$(Atkinson, 1997)
sCI + H_2O → HAHP	$1.0 \times 10^{-17}\ \frac{cm^3}{molecule\cdot s}$
sCI + pinonald. → SOZ20	$1000{\cdot}1.0 \times 10^{-17}\ \frac{cm^3}{molecule\cdot s}$
sCI + NO → pinonald. + NO_2	$610{\cdot}1.0 \times 10^{-17}\ \frac{cm^3}{molecule\cdot s}$
sCI + NO_2 → nitrates	$61{\cdot}1.0 \times 10^{-17}\ \frac{cm^3}{molecule\cdot s}$
sCI + CO → pinonald. + CO_2	$8{\cdot}1.0 \times 10^{-17}\ \frac{cm^3}{molecule\cdot s}$
sCI + SO_2 → org. sulfate	$170{\cdot}1.0 \times 10^{-17}\ \frac{cm^3}{molecule\cdot s}$
sCI + HCOOH → HPAA	$17000{\cdot}1.0 \times 10^{-17}\ \frac{cm^3}{molecule\cdot s}$
sCI + pinic acid → HPAA	$17000{\cdot}1.0 \times 10^{-17}\ \frac{cm^3}{molecule\cdot s}$
sCI + pinonic acid → HPAA	$14000{\cdot}1.0 \times 10^{-17}\ \frac{cm^3}{molecule\cdot s}$
sCI + aldehydes → SOZ	$1000{\cdot}1.0 \times 10^{-17}\ \frac{cm^3}{molecule\cdot s}$
sCI + ketones → SOZ	$70{\cdot}1.0 \times 10^{-17}\ \frac{cm^3}{molecule\cdot s}$
sCI + sCI → SOZ20	$9.2 \times 10^{-14}\ \frac{cm^3}{molecule\cdot s}$ (RO_2 + RO_2 for α-pinene Jenkin et al., 1997)
HAHP→ pinonald. + H_2O_2	$0.00833\ s^{-1}$ (Großmann, 1999)
HAHP + OH → pinonic acid + (NO_2 - NO)	$5.5 \times 10^{-12}\ \frac{cm^3}{molecule\cdot s}$ (Master Chemical Mechanism (MCM) v3.1, 2007)
SOZ20 → sCI + pinonald.	$0.233\ s^{-1}$ (estimation)
SOZ → sCI + aldehydes	$0.233\ s^{-1}$ (estimation)
SO_2 + O^1D → SO_3	$4.3 \times 10^{-32} \cdot \exp(-1000/T) \cdot [M]$ (Master Chemical Mechanism (MCM) v3.1, 2007)
SO_2 + OH → HSO_3	$1.06 \times 10^{-12}\ \frac{cm^3}{molecule\cdot s}$ (Master Chemical Mechanism (MCM) v3.1, 2007)
HSO_3 (+M) → SO_3 + HO_2	$9.2 \times 10^{-14}\ \frac{cm^3}{molecule\cdot s}$ (Master Chemical Mechanism (MCM) v3.1, 2007)
SO_3 + H_2O → H_2SO_4	$3.9 \times 10^{-41} \times 10^{-14}\ \frac{cm^6}{molecule^2\cdot s} \cdot [H_2O]$ (Jayne et al., 1997)
SO_3 + methanol →	$1.64 \times 10^{-14}\ \frac{cm^3}{molecule\cdot s}$ (Master Chemical Mechanism (MCM) v3.1, 2007)

Table 3. Boiling points T_b and vaporization entropies ΔS_{vap} for used for the oxidation products considered in this study.

compound	T_b [K]	ΔS_{vap} $\left[\text{Jmol}^{-1}\text{K}^{-1}\right]$
pinic acid	612	90.2
pinonic acid	569	89.8
LAPHYD	588	90.0
HAPHYD	544	90.0
HAHP	615	90.0
HPAA	616	90.0
SOZ (large)	670	90.0
SOZ (small)	564	90.0
nitrates	522	90.0
PAN type	541	90.0
pinonaldehyde	510	89.3
norpinonaldehyde	491	89.3
CC6CHO	540	89.3

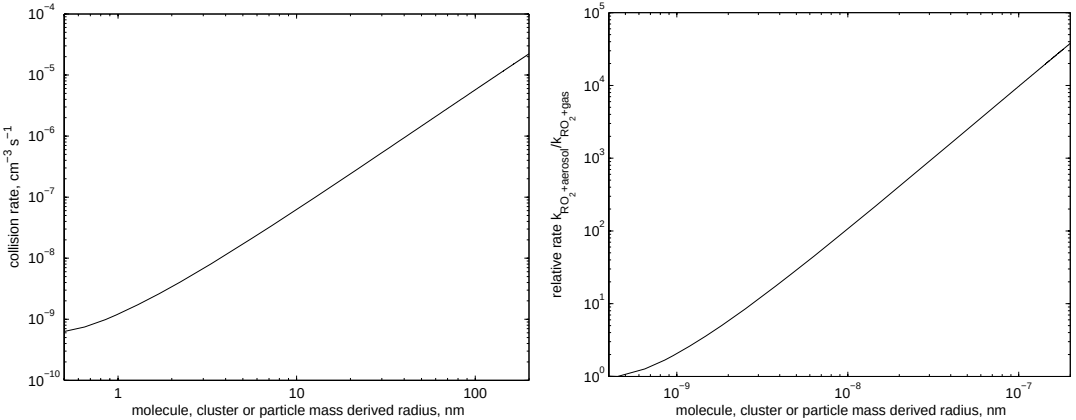

Fig. 1. Displayed in the upper plot is the increase in collision rate of an organic peroxy radical (M = 185 g mol^{-1}) with aerosol particles of different sizes and densities (1200 kg m^{-3}).The lower plot shows the relative reaction rate constant with increasing aerosol size assuming the steric factor to be identical to the gas phase reaction.

ACPD
7, 3901–3939, 2007

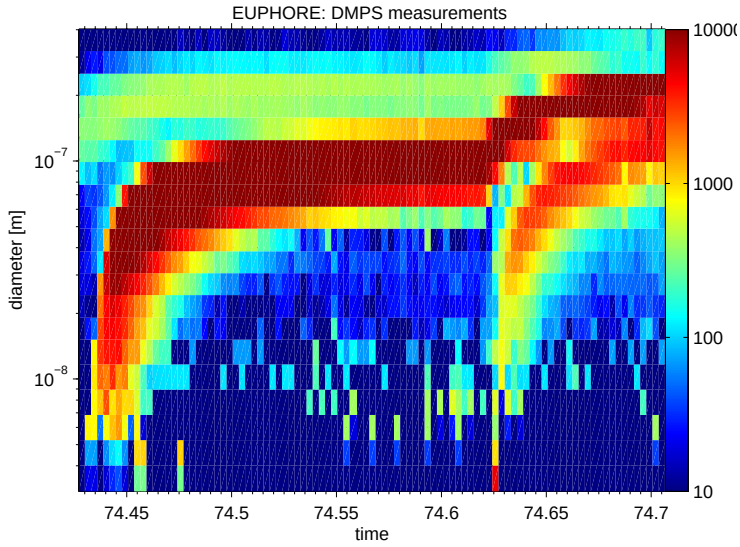

Fig. 2. Shown are the aerosol particle size distribution measurements performed in the α-pinene experiment in the EUPHORE smog chamber facility with a DMPS system.

ACPD
7, 3901–3939, 2007

EGU

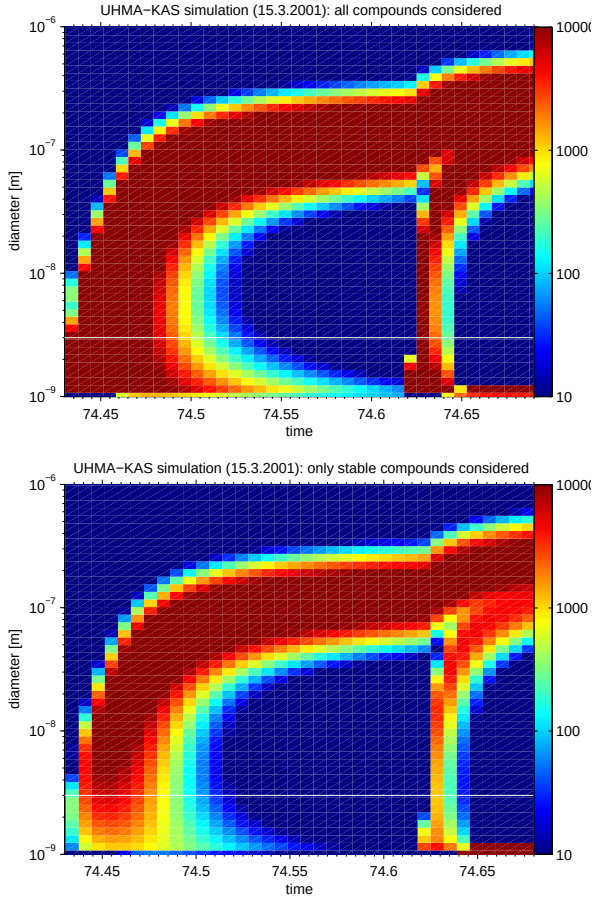

Fig. 3. Simulations performed with UHMA-KAS: the left plot displays the "real" particle size distribution evolution (all compounds considered) simulated and the right one considers only the stable compounds part.

ACPD
7, 3901–3939, 2007

EGU

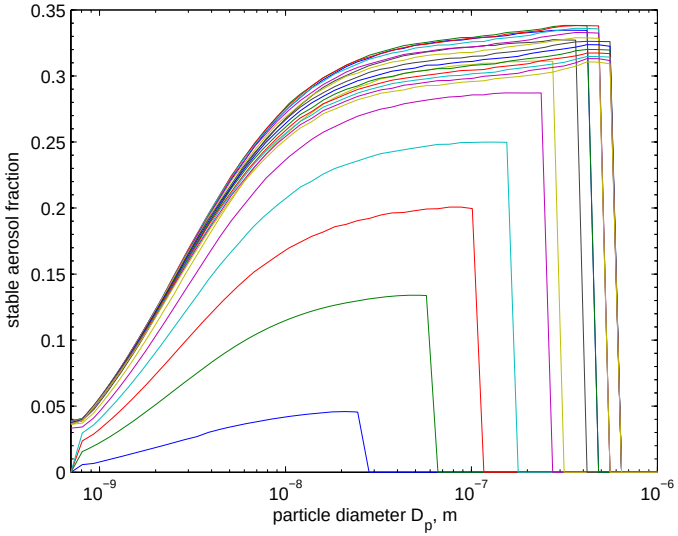

Fig. 4. Simulations performed with UHMA-KAS: displayed is the stable fraction of the simulated aerosol particles in dependence on particle diameter. The different lines show the first 20 time steps (identical to DMPS measurement time steps) after the start of nucleation. The break off at larger diameters is caused by no available aerosol. A stable fraction seems to be reached close to 10 nm.

ACPD
7, 3901–3939, 2007

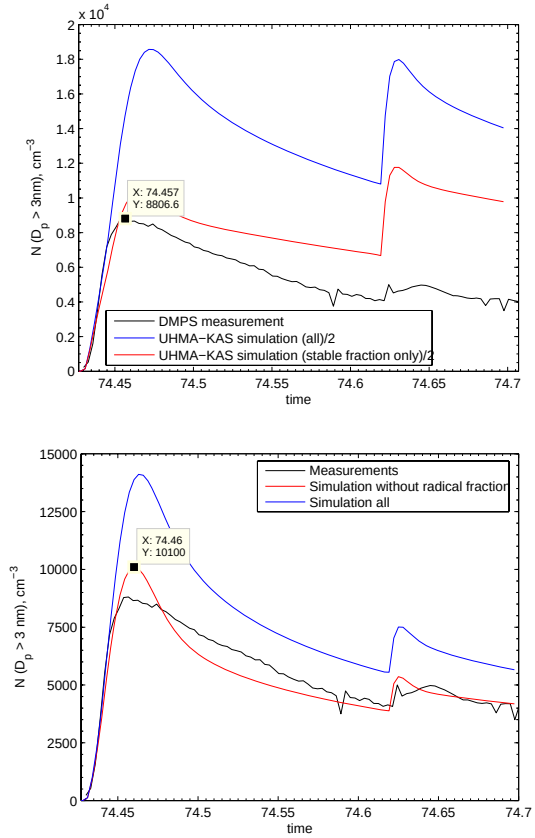

Fig. 5. Comparison of the number concentrations measured (DMPS data, black) and simulated (UHMA-KAS). The simulated are shown including (blue) and excluding the reactive fraction. In the upper plot the situation is shown for the actually measured α−pinene concentrations. In the lower plot the initial injection of α-pinene is increased to 11.5 ppbv and the simulated total number concentration is divided by 6.

ACPD
7, 3901–3939, 2007

EGU

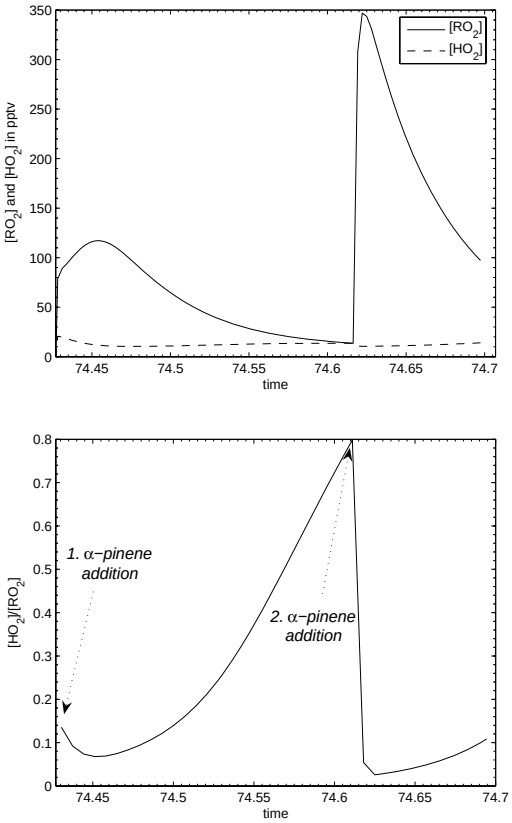

Fig. 6. Chemistry calculations performed with UHMA-KAS. Upper plot: the time evolution of the present peroxy radical volume mixing ratios in pptv. Lower plot: Ratio of HO_2 and RO_2 throughout the experiment. The times of the two α−pinene additions are indicated in both figures by arrows.

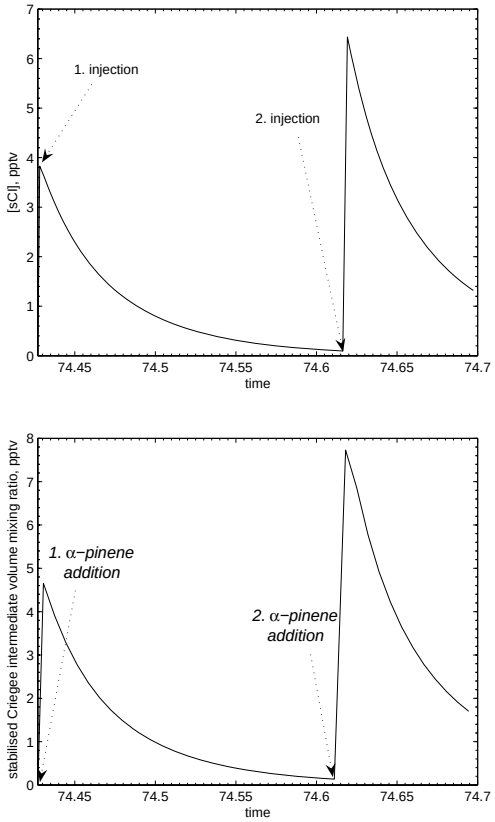

Fig. 7. Calculations of the stabilised Criegee intermediates concentration with time. They are the precursor of the nucleation nuclei. Upper plot: using the actual measured α-pinene concentration, lower plot: both monoterpene injections enhanced by 30%.

ACPD
7, 3901–3939, 2007